Journal of Materials Science and Engineering A 13 (1-3) (2023) 13-25
doi: 10.17265/2161-6213/2023.1-3.002

Effect of Dynamic Strain Aging on Hardness in the Heat-Affected Zone of SUS316 Steel Welds

Lina Yu, Kazutoshi Nishimoto and Kazuyoshi Saida
Graduate School of Engineering, Osaka University, Osaka 565-0871, Japan

Abstract: DSA (dynamic strain aging) phenomenon in SUS316 steel was investigated using isothermal and non-isothermal tensile tests of simulated HAZ (heat-affected zone) thermal cycles. Isothermal tensile tests were performed on SUS316 in the peak temperature range of 20-700 °C, with strain rates varying from 4.2×10^{-3} to 4.2×10^{-5} s^{-1}. Based on the appearance of discontinuous plastic flows, expressed as serrations, and the hardening phenomenon of the tensile samples, the conditions for the occurrence of DSA in the SUS316 steel were investigated. Furthermore, the extent of hardening due to DSA was evaluated by comparing the hardness values of the SUS316 and SUS316EHP steels after the tensile tests. To confirm the effect of DSA on hardness in the HAZ of the welded SUS316 steel, non-isothermal tensile tests of the simulated HAZ thermal cycles were performed using a Thermec Master. The relationship between the increase in Vickers hardness due to DSA and the strain in the HAZ was determined; the effect of DSA on hardness in the HAZ could be predicted. The DSA in SUS316 steel was found to be mainly attributed to the dynamic interaction of dislocations with C and N interstitial atoms during high-temperature deformation.

Key words: Dynamic strain aging, hardness, serration, heat-affected zone, SUS316.

1. Introduction

Austenitic stainless steel SUS316 has excellent high-temperature strength and toughness; therefore, it is widely used in various equipment, such as industrial machinery, nuclear power plants, and marine development equipment. Welding technology is indispensable for constructing large-scale structures. However, after multipass welding, the hardness in the HAZ (heat-affected zone) increases locally, and the stress/strain distribution in the HAZ tends to become nonuniform, which causes serious problems, such as brittle fracture and SCC (stress corrosion cracking) [1-4]. The hardening phenomenon in the HAZ after multipass welding is mainly caused by work hardening owing to tensile deformation and solidification shrinkage during welding. Additionally, DSA (dynamic strain aging) has been suggested as a factor in the hardening phenomenon in the HAZ of austenitic stainless steel welds [5]. Kako et al. reported an increase in the hardness to a value in the range of approximately 30 to 50 HV when the tensile strain was approximately 30%, after an isothermal tensile test of SUS316L steel [6]. The maximum strain observed in the multilayer welded HAZ was reported to be approximately 20%-25% [7, 8]; therefore, the influence of DSA on the hardness of HAZ of SUS316 welds cannot be ignored.

DSA is a phenomenon caused by the interaction between solute atoms and dislocations, which results from the recurring formation of Cottrell atmospheres of solute atoms that act as pinning species. These may be the interstitial or substitutional atoms of alloying elements. The aging of dislocations increases the stress required for their movement during plastic deformation [9]. Owing to the rapid change in deformation stress, the dislocation density and strain hardening rate increase, resulting in a serrated flow on the macroscopic stress-strain curves (i.e., Portevin-Le Châtelier effect) [10]. Owing to the requirement of thermal activation for diffusion and the overcoming of localized obstacles by arrested dislocations, the occurrence of DSA is highly

Corresponding author: Lina Yu, Ph.D., associate professor, research fields: materials science and engineering.

temperature-sensitive [11, 12]. The strain rate also influences DSA by controlling the waiting time of dislocations at localized obstacles [13].

Therefore, in the present study, the effect of DSA on the hardness of SUS316 stainless steel was investigated based on high-temperature isothermal tensile test results obtained over wide temperature andstrain rate ranges. In addition, the strain rate in the HAZ of the weld was much higher than that in the high-temperature tensile test; therefore, to simulate the same strain rate in the HAZ, a Thermec Master (high-temperature deformation simulator) was used in this study. Based on the hardness results, the effect of DSA on the hardness in the HAZ of the SUS316 welds was clarified. Furthermore, the mechanism responsible for DSA in SUS316 steel was elucidated.

2. Materials and Methods

2.1 Materials

In this study, low-carbon austenitic stainless steel SUS316 was used as the base material, and high-purity materials SUS316EHP and SUS304EHP were used for comparison. The chemical compositions of the steels are listed in Table 1.

2.2 Isothermal Tensile Test Using a High-Temperature Tensile Tester

To investigate the DSA behavior of SUS316 steel, isothermal tensile tests were performed using ahigh-temperature tensile tester at a wide temperature range of 20-700 °C, and the strain rates were varied from 4.2 × 10^{-3} to 4.2 × 10^{-5} s^{-1}. To prevent the sample from oxidation, the tests were performed in an atmosphere of 95% argon and 5% hydrogen. The shape and size of the tensile specimens are depicted in Fig. 1.

2.3 Non-isothermal Tensile Test of Simulated HAZ Thermal Cycle Using Thermec Master

The actual strain rate in the HAZ of the weld was much faster than that in the isothermal tensile test; therefore, to simulate the same strain rate in the HAZ, a Thermec Master (high-temperature deformation simulator) was used in this study. The shape and size of the tensile specimen used for the Thermec Master are shown in Fig. 2. To simulate the thermal cycle in HAZ, the heating rate was set to 50 °C/s, and the cooling rates were varied from 30 to 100 °C/s, with the peak temperature set at 500 °C. The maximum strain was set to 30% or 20%, with the strain rate varied from 5.4 × 10^{-2} to 1.8 × 10^{-1} s^{-1}. For comparison, tensile tests were

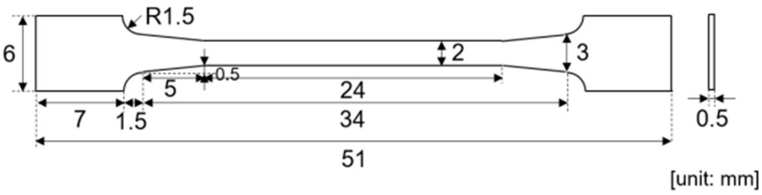

Fig. 1 Tensile specimen for high-temperature tensile tester.

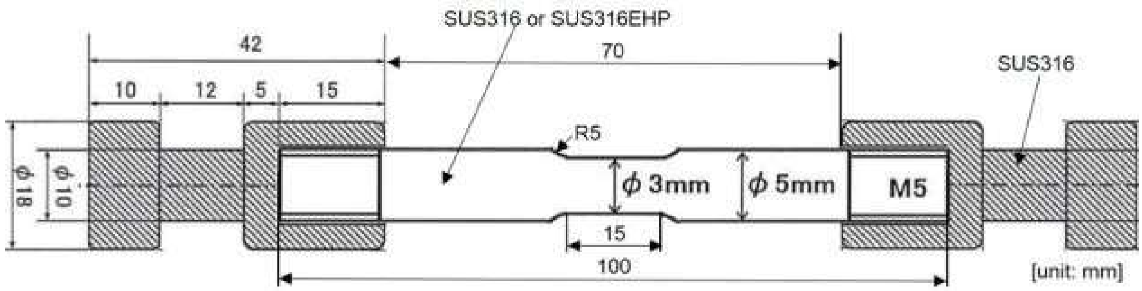

Fig. 2 Tensile specimen for Thermec Master.

Table 1 Chemical compositions (mass %).

Material	C	Si	Mn	P	S	Ni	Cr	Mo	Co	Al	N	O	Fe
SUS316	0.04	0.60	0.93	0.034	0.004	10.16	16.83	2.06	0.20	-	-	-	Bal.
SUS316EHP	0.0018	<0.01	<0.01	0.0008	<0.0005	16.05	16.08	2.05	-	0.022	0.0007	0.0015	Bal.
SUS304EHP	0.0024	<0.01	<0.01	0.0009	<0.0005	15.03	18.06	-	-	0.008	0.0007	0.0027	Bal.

also performed at room temperature for both the SUS316 and SUS316EHP steels. The tests were carried out in an atmosphere of 100% nitrogen to prevent oxidation of the specimen.

2.4 Vickers Hardness Measurement

Vickers hardness tests were conducted to examine changes in hardness after the tensile tests. After polishing, the Vickers hardness at the center of the tensile specimen was measured under a load of 0.098 N for 15 s, and the average value, excluding the maximum and minimum values, was obtained from multiple measurements.

3. Results and Discussion

3.1 DSA Phenomenon in SUS316 Steel

To clarify the occurrence of the DSA phenomenon during high-temperature deformation in SUS316 steel, isothermal tensile tests were carried out at the temperatures of 500 and 20 °C, with a strain rate of 4.2 × 10^{-5} s^{-1}. The maximum strains were set to 20% and 30%, and the obtained stress-strain curves are shown in Fig. 3. Obvious discontinuous plastic flow expressed as serration was discernible in the stress-strain curves recorded at a high temperature of 500 °C with maximum strains of both 20% and 30% in the SUS316 steel. By contrast, no serration was observed in the stress-strain curves recorded at room temperature. These results suggest that DSA only occurs during the tensile deformation of SUS316 steel at high temperatures.

The hardness at the center of the tensile specimen at 500 and 20 °C was measured, and the relationship between Vickers hardness and plastic strain is presented in Fig. 4. Compared with the hardness after the tensile test at 20 °C, higher hardness values were observed in the tensile specimen analyzed at 500 °C, with an increase of approximately 40 HV at the maximum strain of 30%. This indicates that DSA during high-temperaturedeformation has a remarkable effect on the hardness of SUS316 steel.

For comparison, tensile tests were also performed for the high-purity steels SUS316EHP and SUS304EHP at a temperature of 500 °C with a maximum strain of 20%. Fig. 5 shows the recorded stress-strain curves for the three types of steel. Serration was not observed in the stress-strain curve of the SUS304EHP steel; however, remarkable serration was observed in the stress-strain curve of the SUS316 steel. In addition, few serrated flows were found in the stress-strain curve of the SUS316EHP steel. Overall, the DSA phenomenon occurs during the tensile deformation of SUS316 steel at high temperatures.

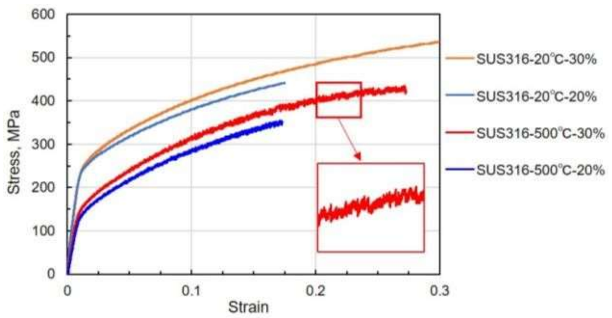

Fig. 3 Stress-strain curves recorded at 20 and 500 °C with different strains in SUS316 steel.

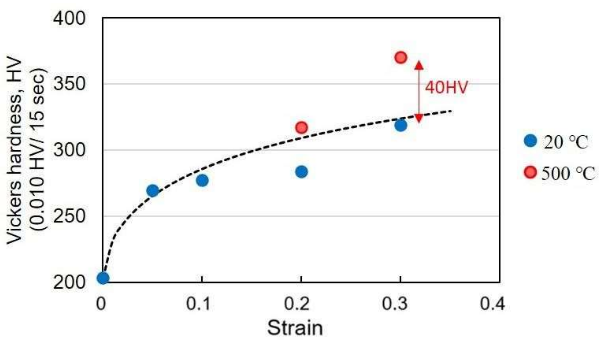

Fig. 4 Relationship between Vickers hardness and tensile strain at 20 and 500 °C in SUS316 steel.

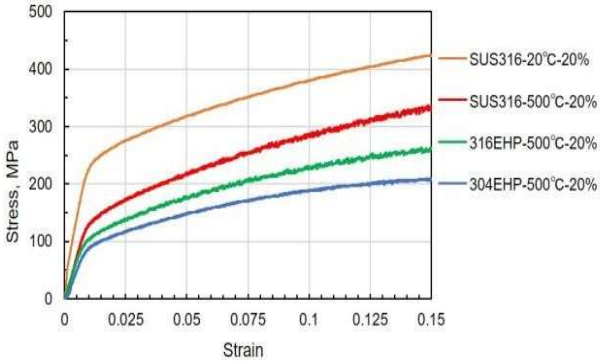

Fig. 5 Stress-strain curves of SUS316, SUS316EHP, and SUS304EHP.

3.2 Occurrence Conditions of DSA in SUS316 Steel by Isothermal Tensile Test

The maximum strain observed in the multilayer welded HAZ is approximately 20% to 25% [7, 8]; therefore, in the present study, the occurrence conditions of DSA in SUS316 steel were investigated mainly by isothermal tensile tests with a maximum strain of 20% at different peak temperatures and strain rates.

3.2.1 Stress-Strain Curves of Isothermal Tensile Tests

The stress-strain curves for the SUS316 tensile specimens tested in the temperature range of 20-700 °C with the strain rates varied from 4.2×10^{-3} to 4.2×10^{-5} s^{-1} are illustrated in Figs. 6-8, respectively. Fig. 6a shows the stress-strain curves for uniaxial tensile tests up to fracture at a high strain rate of 4.2×10^{-3} s^{-1}, and Fig. 6b presents a magnified view of stress-strain curve portions in the strain range of 12%-17%. The occurrence of discontinuous plastic deformation is obvious in the serrated deformation curves for 500 and 700 °C. When the strain rate is changed to 4.2×10^{-4} s^{-1}, as shown in Fig. 7, remarkable serrated flow can be observed in the stress-strain curves for 500 and 600 °C. However, at a low strain rate of 4.2×10^{-5} s^{-1}, as presented in Fig. 8, serration is evident even in the stress-strain curve for 300 °C. These results indicate that at a lower strain rate, discontinuous plastic deformation occurs more easily in SUS316 steel. Further, serrated flow occurred mostly in the temperature range from 300 °C to 600 °C.

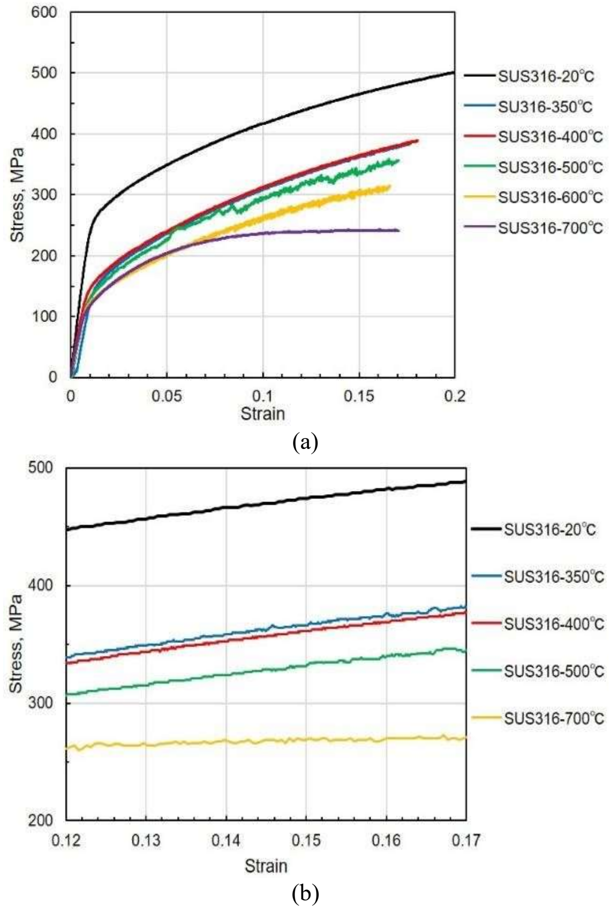

Fig. 6 Stress-strain curves of SUS316 tensile specimens recorded at different temperatures with the strain rate of 4.2×10^{-3} s^{-1}: (a) Stress-strain curves for uniaxial tensile tests up to fracture and (b) a magnified view of portions of the curves in (a) to assess the occurrence of serrated flow.

3.2.2 Hardness Results of Isothermal Tensile Test Specimens

The SUS316 and SUS316EHP samples were subjected to 20% isothermal tensile tests at room temperature and high temperatures, following which Vickers hardness measurements were performed at the center of the tensile specimen, and the corresponding values are presented in Fig. 9. The hardness of the base metal (ST (solution treatment)) for both SUS316 and SU316EHP was approximately 200 HV, as indicated by the dotted line in Fig. 9. Compared with the hardness at room temperature, the hardness after high-temperature tensile tests increased significantly, indicating that the strain hardening caused by DSA has occurred in SUS316 steel, with the highest hardness value at

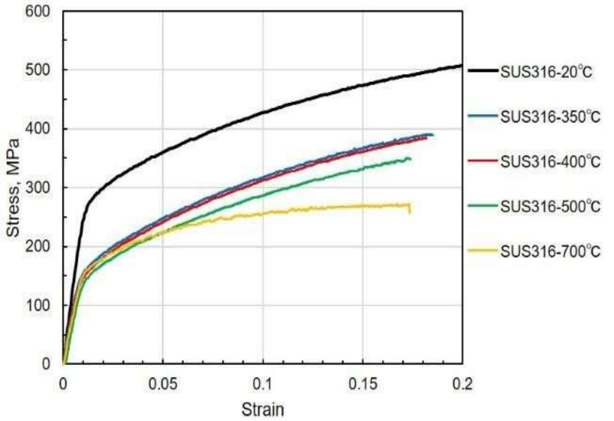

(a)

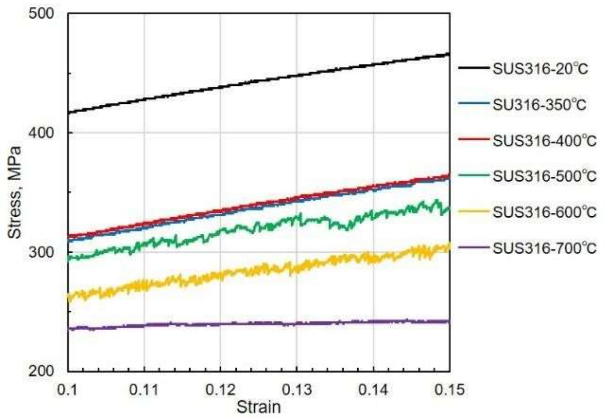

(b)

Fig. 7 Stress-strain curves of SUS316 tensile specimens recorded at different temperatures with the strain rate of 4.2 × 10^{-4} s^{-1}: (a) Stress-strain curves for uniaxial tensile tests up to fracture and (b) a magnified view of portions of the curves in (a) to assess the occurrence of serrated flow.

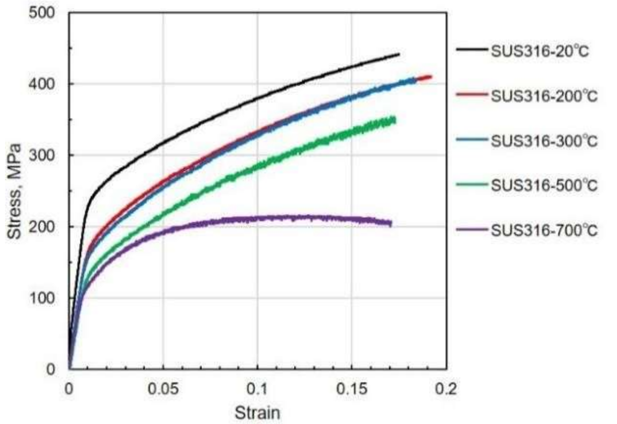

(a)

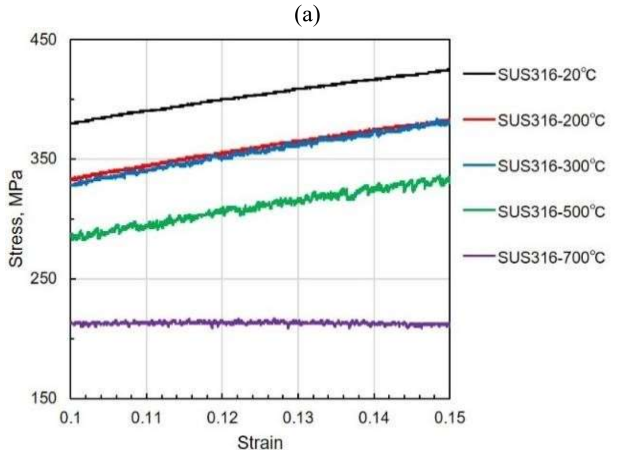

(b)

Fig. 8 Stress-strain curves of SUS316 tensile specimens recorded at different temperatures with the strain rate of 4.2 × 10^{-5} s^{-1}: (a) Stress-strain curves for uniaxial tensile tests up to fracture and (b) a magnified view of portions ofthe curves in (a) to assess the occurrence of serrated flow.

500 °C at any strain rate. In addition, at all strain rates, a softening phenomenon was observed at 700 °C, which is possibly due to recovery or recrystallization at the high temperature. However, for the SUS316EHP steel, the hardness values after the tensile test at high temperatures were almost the same as those at room temperature. This suggests that impurity elements, such as C and N, in SUS316 steel have a significant effect on the DSA.

The extent of hardening due to DSA in SUS316 steel was investigated from the hardness results after the isothermal tensile test. Fig. 10 shows a schematic of the method used to examine the extent of hardening due to DSA. The hardness values of the SUS316 and SUS316EHP steels after the room-temperature tensile tests were different, as shown in Fig. 9. This is attributed to the presence of impurity elements in the SUS316 steel; therefore, the effect of impurity elements on hardening can be investigated by considering the hardness difference between the two steels. After the high-temperature tensile test of SUS316, in addition to the work hardening and hardening due to impurity elements observed in the room-temperature tensile test, hardening due to DSA and softening due to recovery during the cooling process occurred simultaneously. By contrast, for the SUS316EHP steel, only work hardening and softening owing to recovery during the cooling process occurred after the high-temperature tensile test. Therefore, based on the hardness difference between SUS316 and

SUS316EHP after the high-temperature tensile test, the hardening due to DSA and the presence of impurity elements can be examined. Furthermore, by subtracting the hardness difference between SUS316 and SUS316EHP after the room-temperature tensile test fromthis difference, the hardening due to DSA can be confirmed.

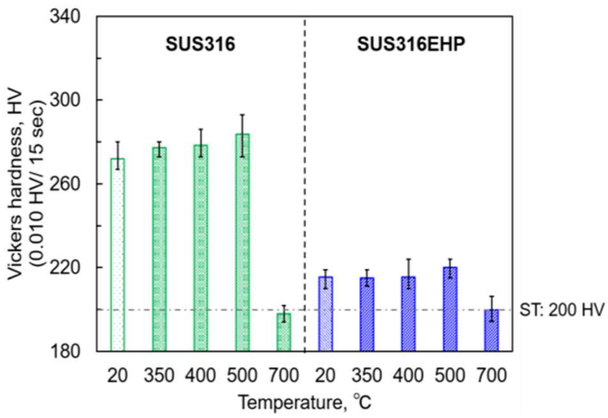

(a)

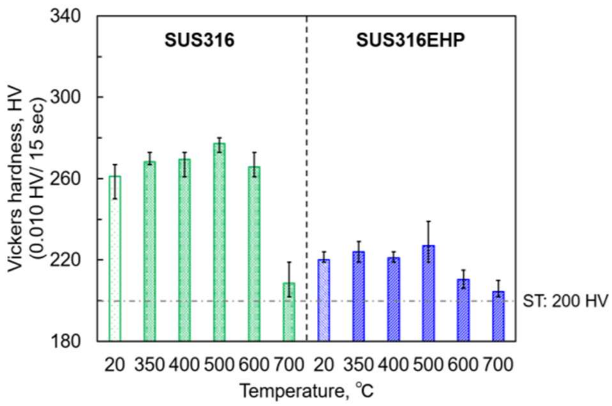

(b)

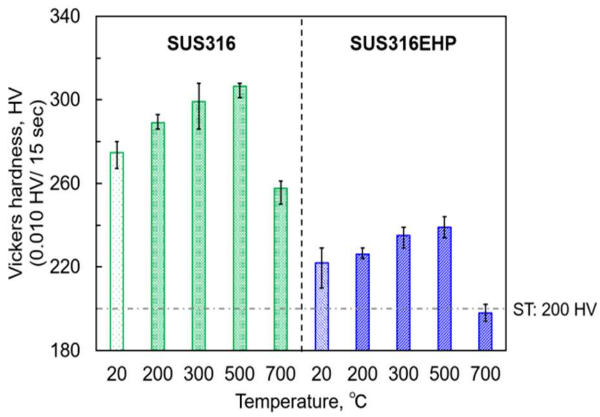

(c)

Fig. 9 Relationship between peak temperature and Vickers hardness at 20-700 °C for strain rates of (a) 4.2 × 10^{-3} s^{-1}, (b) 4.2 × 10^{-4} s^{-1}, and (c) 4.2 × 10^{-5} s^{-1}.

		Work hardening	Effect of impurity elements	Dynamic strain aging	Recovery
Room temperature	SUS316	○	○		
	SUS316EHP	○			
High temperature	SUS316	○	○	○	○
	SUS316EHP	○			○

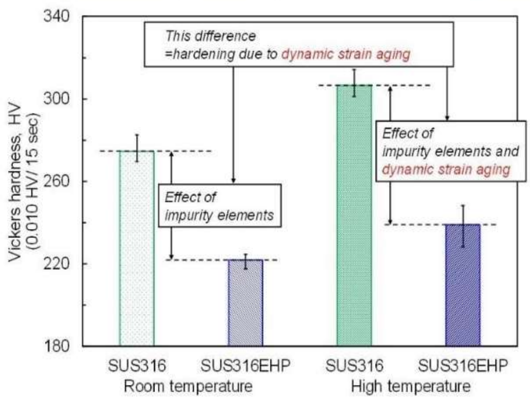

Fig. 10 Schematic of the method employed to study hardening due to DSA.

Table 2 Hardening due to DSA in SUS316 steel at different. strain rates

Strain rate/s^{-1}	Temperature/°C	ΔHV
4.2 × 10^{-3}	350	5.8
	400	6.4
	500	7.2
4.2 × 10^{-4}	350	3.0
	400	7.2
	500	9.0
	600	14.2
4.2 × 10^{-5}	200	10.2
	300	11.4
	500	14.8

The extents of hardening due to DSA in SUS316 steelat different strain rates are listed in Table 2 and suggest that the hardening due to DSA was affected by both the peak temperature and strain rate. The hardening was maximum in the peak temperature range of 500-600 °C and increased with decreasing strain rates.

3.2.3 Occurrence Conditions of DSA in SUS316 Steel

Based on the serration phenomenon observed in the stress-strain curve and the hardening due to DSA, the conditions for DSA in SUS316 steel were investigated. These are summarized in Fig. 11, which were determined by both the peak temperatures and the strain rates. On the low-temperature side, DSA hardening was observed

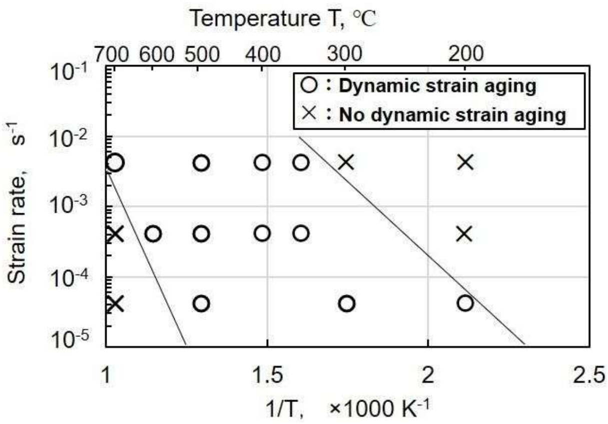

Fig. 11 Strain rate and temperature dependencies of DSA hardening conditions in SUS316 steel.

even under conditions in which serrations were not observed. This suggests that the DSA phenomenon had occurred but not to an extent where serrations could be clearly observed. However, because the effect of recovery on hardness is greater at higher temperatures, it is difficult to determine the occurrence of DSA solely from the hardness values. Therefore, the conditions for DSA in SUS316 steel were determined by the occurrence of serrations on the high-temperature side and hardness on the low-temperature side. Furthermore, with decreasing strain rate, the conditions for DSA to ensue became wider, indicating that DSA occurred easily at low strain rates. The DSA phenomenon may ensue mainly under the conditions corresponding to the region between the two straight lines in Fig. 11 for SUS316 steel.

3.3 Hardening by DSA in Simulated HAZ of SUS316 Steel Welds

A schematic of the thermal and strain histories in the actual welding HAZ is shown in Fig. 12b, along with those of the isothermal tensile tests (Fig. 12a) discussed in Section 3.2. In the actual HAZ, strain occurred in a non-isothermal process during the cooling process, and the strain rate was assumed to be significantly higher than that in the isothermal tensile test. Therefore, to confirm the hardening by DSA in the HAZ, the high-temperature tensile tests should be performed under conditions similar to the strain behavior of actual HAZ, and thus, a Thermec Master (high-temperature deformation simulator) was used.

Regarding the test conditions of the Thermec Master, the peak temperature was set at 500 °C, because the maximum hardening was determined as ~500 °C in the previous isothermal tensile tests. The cooling rates were set to 30 and 100 °C, which are usual in the actual welding HAZ. The previous studies showed that the maximum strain observed in the multilayer welded HAZ is approximately 20% to 25% [7, 8], and there is almost no DSA hardening when the strain is lower than 10% [6]. Therefore, in this study, the maximum strain amounts were set to 20% and 30% for non-isothermal tensile tests using the Thermec Master. The tensile strain was applied during the cooling process from 500 °C to 300 °C. For comparison, tensile tests were performed at room temperature to confirm the extent of hardening caused by DSA.

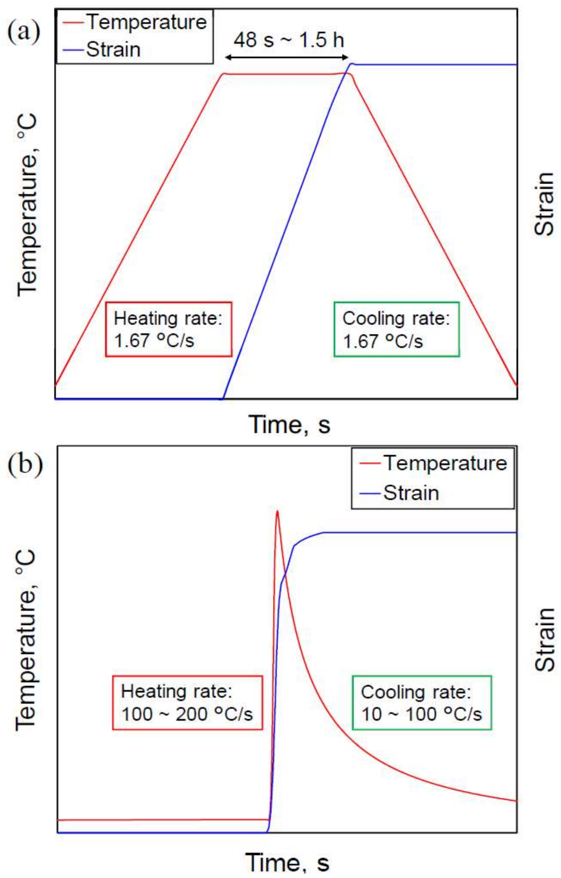

Fig. 12 Comparison of thermal and strain histories of (a) the isothermal tensile test and (b) actual welding HAZ.

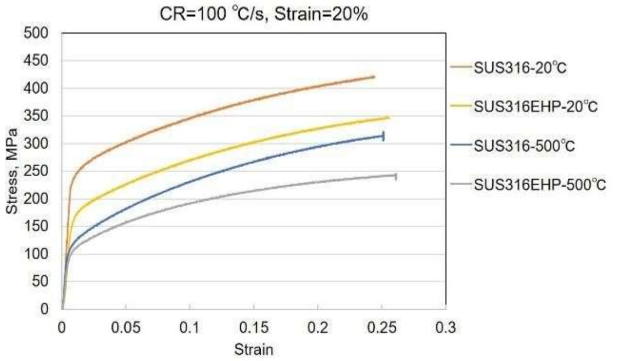

(a)

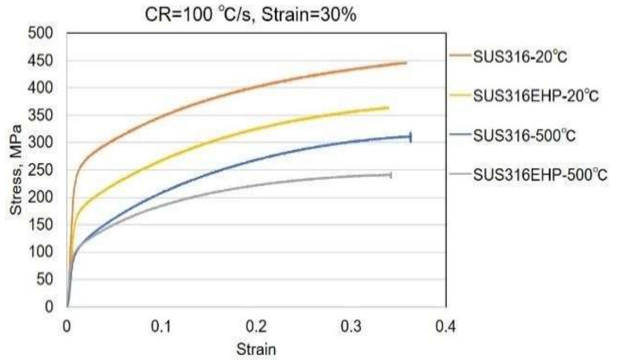

(b)

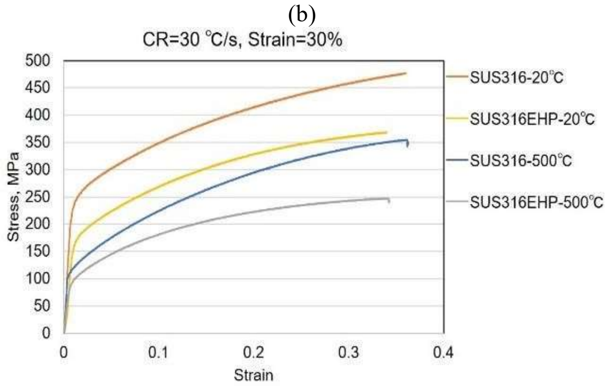

(c)

Fig. 13 Stress-strain curves of SUS316 and SUS316EHP steels: (a) CR = 100 °C/s, Strain = 20%, (b) CR = 100 °C/s, Strain = 30%, and (c) CR = 30 °C/s, Strain = 30%.

The stress-strain curves of the simulated HAZ thermal cycle using the Thermec Master for both SUS316 and SUS316EHP steels are illustrated in Fig. 13. No serration was observed in the stress-strain curves, which may be due to the high strain rate. Fig. 14 shows the hardness values measured after the tensile tests. Under all conditions, the hardness values after the tensile test at 500 °C were lower than those after the tensile test at room temperature, suggesting that the effect of softening due to recovery was much greater than the effect of hardening due to DSA at 500 °C.

Based on the hardness results in Fig. 14, the relationship between the strain and hardening due to the DSA of the simulated HAZ thermal cycle is summarized in Fig. 15. For a strain of 30%, the average hardness values for cooling rates of 30 and 100 °C/s were plotted. From this result, it was found that the maximum hardening owing to DSA was approximately 12.5 HV when a strain of 30% was applied in HAZ, and the hardening by DSA was approximately 5.5 HV at a strain of 20%. The relationship between the increase in Vickers hardness due to DSA and the strain in HAZ can be expressed as Eq. (1) when the strain is higher than 10%. Using this method, the increase in the Vickers hardness due to DSA can be predicted when the strain in the HAZ is known.

$$\Delta HV = 61\varepsilon - 6 \tag{1}$$

3.4 Mechanism of DSA Occurrence in SUS316

According to the pioneering work of Cottrell [14, 15], regions of increased solute concentration can form around dislocations, known as Cottrell atmospheres. The motion of a dislocation distorts its Cottrell atmosphere, resulting in a drag force on the moving dislocation. The dislocations that break away from the Cottrell atmospheres produce a burst of plastic strain. If solutes are sufficiently mobile to maintain pace with moving dislocations, Cottrell atmospheres can repeatedly reform during a dislocation glide when the mobile dislocations are temporarily arrested at localized obstacles [16].

A generally accepted explanation for the discontinuous plastic flow in the stress-strain curve is the DSA effect [17], which is caused by the recurring formation of Cottrell atmospheres of solute atoms acting as the pinning species. If the solute atoms are capable of dislocation pinning, the occurrence of DSA depends mainly on the interplay between the waiting time of dislocations at the localized obstacles and the characteristic time for solute diffusion to dislocations temporarily arrested at the localized obstacles [9, 10].

DSA is highly temperature-sensitive because of the requirement of thermal activation for diffusion to overcome localized obstacles [13, 14]. In addition, the strain rate significantly influences the occurrence of DSA by controlling the waiting time of dislocations at the localized obstacles [15]. This explains the isothermal tensile test results shown in Figs. 8 and 9 in Section 3.2.

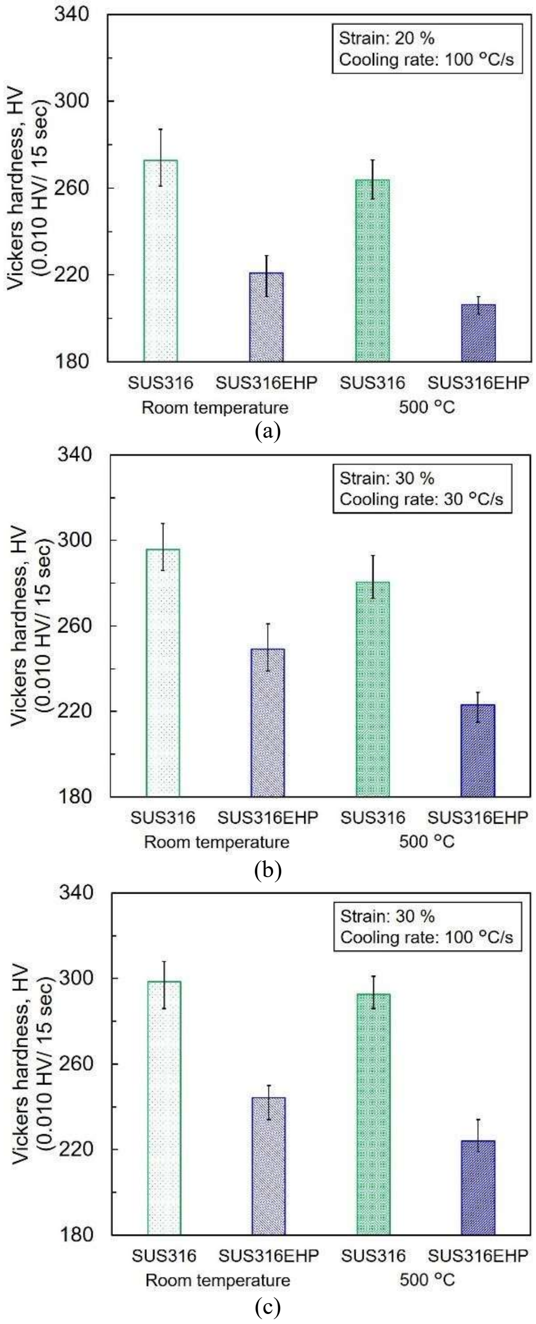

Fig. 14 Comparison of Vickers hardness: (a) CR = 100 °C/s, Strain = 20%, (b) CR = 100 °C/s, Strain = 30%, and (c) CR = 30 °C/s, Strain = 30%.

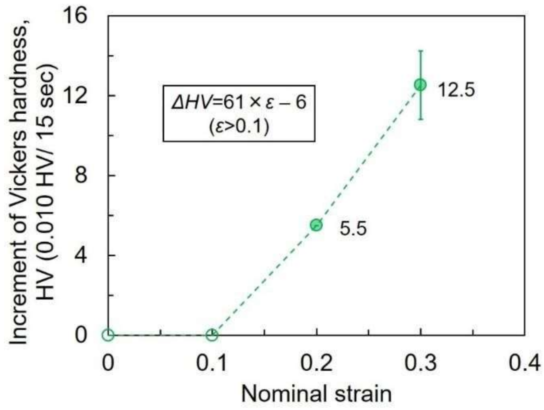

Fig. 15 Increment in Vickers hardness due to DSA in simulated HAZ.

In general, DSA in steel is caused by interstitial atoms (mainly C and N) dissolved in the material that accumulate in dislocations and produce a repeated drag force on the moving dislocation. However, it has also been reported that Mo, which is a substitutional solute atom, promotes DSA [18]. For the SUS316EHP steel used in this study, the hardness values after the high-temperature tensile tests were slightly higher than those after the room-temperature tensile tests, as shown in Fig. 9. This indicates that interstitial as well as substitutional solute atoms may contribute to occurrence of DSA in austenitic stainless steels. Based on the above results, the effects of Cr, Ni, and Mo, which are the main constituent elements of SUS316, and of the impurity elements C and N on DSA hardening are discussed from the viewpoint of the interaction between dislocations andsolute atoms.

Fig. 16 shows a schematic of the stress field around an edge dislocation, where a compressive strain field and a tensile strain field occur in the upper and lower parts, respectively. When the diffusion rate of solute atoms increases in a high-temperature environment, the solute atoms accumulate around the dislocation and relax the unstable stress field around the dislocation. Fig. 17 shows a schematic of the strain field around solute atoms and their interactions with dislocations. As shown in Fig. 17a, C and N are interstitial solute atoms with extremely small atomic radii that generate compressive strain fields around them; thus, they interact with the tensile strain field under the dislocation line. A substitutional solute atom with a large atomic radius such as Mo generates a compressive strain field around it and interacts with the tensile strain field under the dislocation line, as illustrated in Fig. 17b. By contrast, substitutional solid-solution atoms, such as Cr and Ni, whose atomic radii are similar to those of the Fe solvent atoms, are considered to have less strain around them and very little interaction with the dislocations, as shown in Fig. 17c. Interstitial solute atoms, such as C and N, significantly affect the occurrence of DSA in austenitic stainless steel. In addition, the substitutional solute atom, Mo, which has a larger atomic radius than Fe, may also generate DSA because it provides resistance to dislocation movement. However, Cr and Ni, which have atomic radii similar to that of Fe, have very little interaction with dislocations; therefore, their effects on the development of serrations are considered negligible.

For solute atoms to interact with dislocations during high-temperature deformation and provide viscous resistance, the diffusion rate of solute atoms must be sufficiently high compared with the motion rate of dislocations. However, the diffusion rate of substitutional solid-solution atoms, such as Mo, is much slower than that of interstitial solid-solution atoms, which are generally considered to promote DSA. Cottrell discussed the diffusion rate of substitutional solute atoms during deformation in Al alloys, and Mg and Cu substitutional solute atoms were thought to affect the serration development in Al alloys [15, 19]. The diffusion coefficient of substitutional atoms in the equilibrium state is extremely small compared with that of interstitial atoms, which is thought to cause serrations. However, as shown in the schematic in Fig. 18, lattice defects such as vacancies occur during plastic deformation, and these vacancies can increase the diffusion rate of substitutional solute atoms. Therefore, it is possible that vacancies generated during high-temperature deformation accelerate the diffusion rate of Mo to the extent of serration in the SUS316EHP steel.

Based on the above discussion, Figs. 19a and 19b present the schematics of the mechanism of DSA occurrence in SUS316 and SUS316EHP, respectively. For the SUS316 steel, the dislocations and vacancies increase owing to high-temperature deformation, following which the C and N atoms stick to the dislocations owing to the increased diffusion rate of C

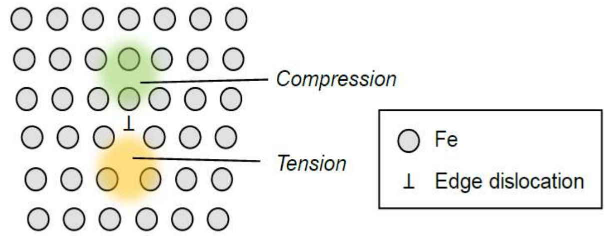

Fig. 16 Schematic of stress field around an edge dislocation.

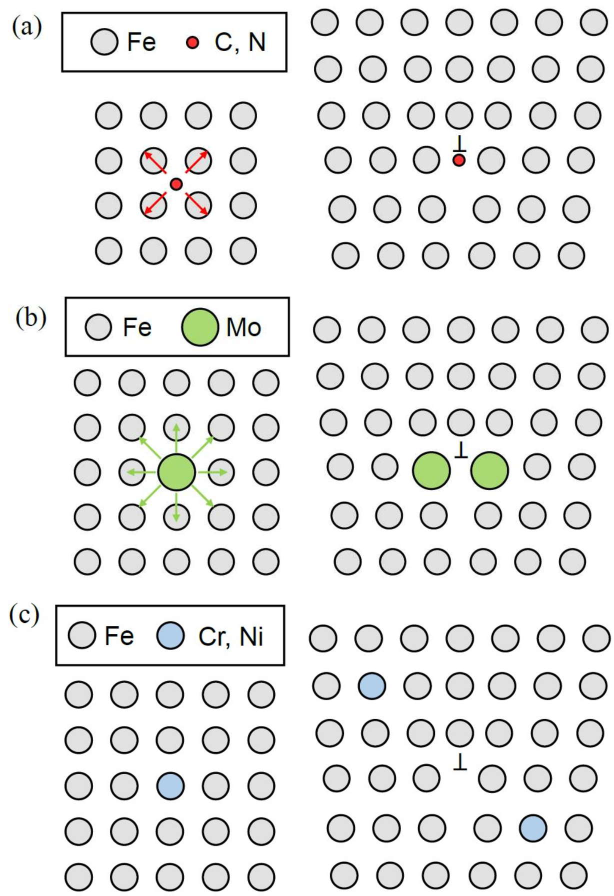

Fig. 17 Schematics of the strain field around solute atoms and their interactions with dislocations: (a) interstitial solid solution (C, N), (b) substitutional solid solution (Mo), and (c) substitutional solid solution (Cr, Ni).

Fig. 18 **Schematic of diffusion of substituted solid solution.**

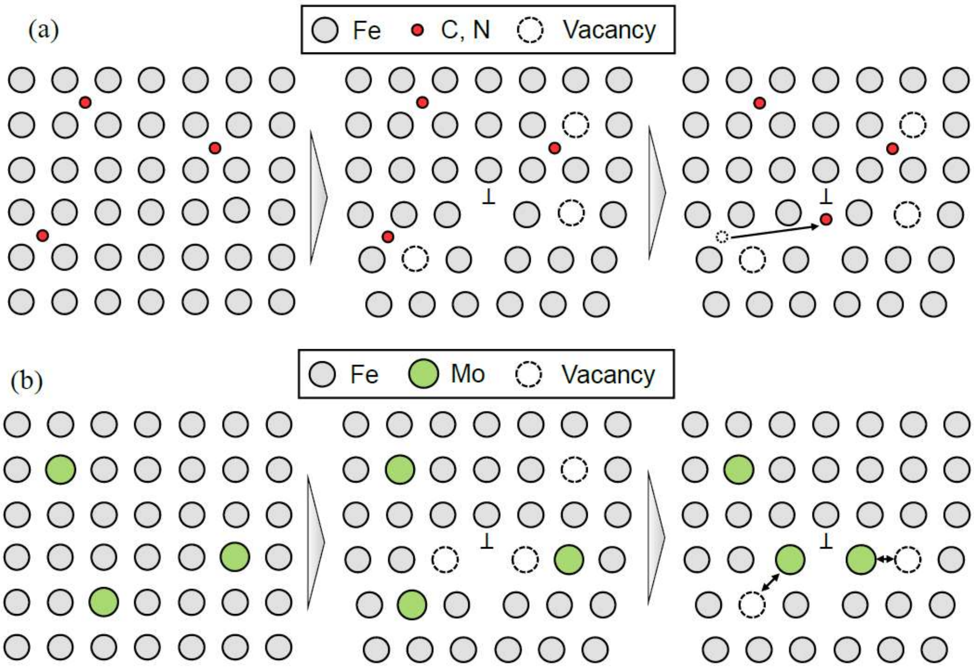

Fig. 19 **Schematics of the mechanism of DSA in (a) SUS316 and (b) SUS316EHP.**

and N in the high-temperature environment. By contrast, in the absence of interstitial solid-solution atoms in SUS316EHP steel, the vacancies introduced by deformation can increase the diffusion rate of Mo, and the Mo atoms attach to the dislocations. The serrations are postulated to be generated by repeating the process in which the solute atoms stick to the dislocations and the dislocations tear off the solute atoms.

In addition, it is well known that Cr and Mo substitutional solute atoms have strong chemical interactions with C and N interstitial solute atoms. In Fe-Cr and Fe-Mo alloys, substitutional solute atoms are reportedly attracted to the vicinity of dislocations by chemical forces, which may affect the motion of dislocations [20]. Therefore, even if Mo alone does not promote DSA, it is possible that Mo affects the DSA in SUS316 because of the chemical interactions between Mo and C/N atoms. However, the possibility that Mo atoms cause DSA in SUS316EHP cannot be ruled out, and its influence is presumed to be small. Based on the above considerations, the hardening due to DSA examined in this study is generally considered appropriate, although the effect of DSA caused by Mo alone is insufficient.

4. Conclusions

In this study, the DSA phenomenon in SUS316 austenite stainless steel was investigated using isothermal and non-isothermal tensile tests of simulated HAZ thermal cycles. The following conclusions were drawn.

(1) Isothermal tensile tests were performed on SUS316 in the peak temperature range from 20 °C to 700 °C, with the strain rates varied from 4.2×10^{-3} to 4.2×10^{-5} s^{-1}. The DSA occurrence conditions were

investigated from the appearance of discontinuous plastic flow expressed as serrations and hardening phenomenon of the tensile samples. The temperature range conducive to the occurrence of DSA can be predicted from the presence or absence of serrations on the high-temperature side and the hardness value on the low-temperature side.

(2) The extent of hardening due to DSA was summarized by comparing the hardness values of the SUS316 and SUS316EHP steels after the tensile tests. Within the DSA occurrence condition, the hardening due to DSA tended to increase with a decrease in the strain rate and an increase in the peak temperature.

(3) To confirm the effect of DSA on the hardness of the HAZ of the welded SUS316 steel, non-isothermal tensile tests of the simulated HAZ thermal cycles were performed using a Thermec Master. It was found that the maximum hardening due to DSA was approximately 12.5 HV when a strain of 30% was applied to the HAZ. The relationship between the Vickers hardness increase due to DSA and the strain in the HAZ was summarized; thus, the effect of DSA on the hardness in the HAZ can be predicted.

(4) The DSA ensuing in SUS316 steel was mainly attributed to the dynamic interaction of dislocations with C and N interstitial atoms during high-temperature deformation.

Acknowledgment

This work was supported by Kansai Electric Power Co., Inc., Japan. The authors gratefully acknowledge the assistance of Mr. Ikumi Asai, who holds a Master's degree from the Graduate School of Engineering, Osaka University, Japan.

References

[1] Meisnar, M., Vilalta-Clemente, A., Moody, M., Arioka, K., and Lozano-Perez, S. 2016. "A Mechanistic Study of the Temperature Dependence of the Stress Corrosion Crack Growth Rate in SUS316 Stainless Steels Exposed to PWR Primary Water." *Acta Mater.* 114: 15-24.

[2] Asadi, P., Alimohammadi, S., Kohantorabi, O., Fazli, A., and Akbari, M. 2020. "Effects of Material Type, Preheating and Weld Pass Number on Residual Stress of Welded Steel Pipes by Multi-pass TIG Welding (C-Mn, SUS304, SUS316)." *Therm. Sci. Eng. Prog*. 16: 100462.

[3] Liu, R.-F., and Wang, J.-C. 2021. "Finite Element Analyses of the Effect of Weld Overlay Sizing on Residual Stresses of the Dissimilar Metal Weld in PWRs." *Nucl. Eng. Des*. 372: 110959.

[4] Tsubota, M., Kanazawa, Y., and Inoue, H. 1995. "Effect of Cold Work on the SCC Susceptibility of Austenitic Stainless Steels." In *Proceedings of 7th International Symposium on Environmental Degradation of Materials in Nuclear Power Systems Water Reactors*, pp. 519-27.

[5] Hong, S. G., and Lee, S. B. 2003. "The Influence of Dynamic Strain Aging on Tensile and LCF Properties of Prior Cold Worked 316L Stainless Steel." *Trans. Korean Soc. Mech. Eng. A*. 27: 1398-408.

[6] Kako, K., Miyahara, Y., Hide, K., and Mayuzumi, M. 2008. "Effects of Temperature and Strain Rate on Dynamic Strain Aging in Heat-Affected Zone of Type 316L Stainless Steel." *Trans. Jpn. Inst. Met*. 72: 206-10.

[7] Barnby, J. T. 1965. "Effect of Strain Aging on the High-Temperature Tensile Properties of an AISI 316 Austenite Stainless Steel." *J. Iron Steel Inst. Jpn*. 203: 392-7.

[8] Kashyap, B. P., McTaggart, K., and Tangri, K. 1988. "Study on the Substructure Evolution and Flow Behavior in Type 316L Stainless Steel over the Temperature Range 21-900 °C." *Philos. Mag. A* 57: 97-114.

[9] De Almeida, L. H., May, I. L., and Emygdio, P. R. O. 1998. "Mechanistic Modeling of Dynamic Strain Aging in Austenitic Stainless Steels." *Mater. Charact*. 41: 137-50.

[10] Mola, J., Luan, G., Huang, Q., Ullrich, C., Volkova, O., and Estrin, Y. 2021. "Dynamic Strain Aging Mechanisms in a Metastable Austenitic Stainless Steel." *Acta Mater*. 212: 116888.

[11] Hong, S.-G., and Lee, S.-B. 2004. "The Tensile and Low-Cycle Fatigue Behavior of Cold Worked 316L Stainless Steel: Influence of Dynamic Strain Aging." *Int. J. Fatigue*. 26: 899-910.

[12] Samuel, K. G., Mannan, S. L., and Rodriguez, P. 1992. "Effect of Ageing on the Strain Rate Sensitivity and Serrated Flow of a Type 316 Stainless Steel at 923 K." *Scr. Metall. Mater*. 26: 685-9.

[13] Kubin, L. P., and Estrin, Y. 1990. "Evolution of Dislocation Densities and the Critical Conditions for the Portevin-Le Chatelier Effect." *Acta Metall. Mater*. 38: 697-708.

[14] Cottrell, A. H., Jaswon, M. A., and Mott, N. F. 1949. "Distribution of Solute Atoms round a Slow Dislocation." *Proc. R. Soc. Lond. Ser. Math. Phys. Sci*. 199: 104-14.

[15] Cottrell, A. H. 1953. "A note on the Portevin Le-Chatelier Effect." *Lond. Edinb. Dublin Philos. Mag. J. Sci.* 44: 829-32.

[16] Sills, R. B., and Cai, W. 2016. "Solute Drag on Perfect and Extended Dislocations." *Philos. Mag*. 96: 895-921.

[17] Yilmaz, A. 2011. "The Portevin-Le Chatelier Effect: A Review of Experimental Findings." *Sci. Technol. Adv. Mater*. 12: 063001.

[18] Kako, K., Miyahara, Y., Arai, T., and Mayuzumi, M. 2009. "Effects of Doped Elements on Material Hardening on the Weld Heat Affected Zone of High-Purity Fe-Cr-Ni Alloy." Report of Electric Power Central Research Institute, Q08021.

[19] Zhang, B., Liaw, P. K., Brechtl, J., Ren, J., Guo, X., and Zhang, Y. 2020. "Effects of Cu and Zn on Microstructures and Mechanical Behavior of the Medium-Entropy Aluminumalloy." *J. Alloys Compd*. 820: 153092.

[20] Monma, K., Suto, H., and Ogita, H. 1965. "On the Chemical Interaction between Interstitial Atoms and Substitutional Atoms Affecting the Strength of Iron-Chromium and Iron-Molybdenum Alloys." *J. Jpn. Inst. Met*. 29: 941-7.